AJNR

Cerebrospinal fluid flow measured by phase-contrast cine MR.

D R Enzmann and N J Pelc

AJNR Am J Neuroradiol 1993, 14 (6) 1301-1307
http://www.ajnr.org/content/14/6/1301

Cerebrospinal Fluid Flow Measured by Phase-Contrast Cine MR

Dieter R. Enzmann and Norbert J. Pelc

PURPOSE: This prospective study was designed to establish the temporal and quantitative relationship between blood flow and cerebrospinal fluid (CSF) flow using a phase-contrast cine MR pulse sequence. **METHODS:** A cine phase-contrast MR pulse sequence using peripheral gating was used to measure CSF flow direction and velocity. Data were acquired continuously and interpolated into 16 images throughout the cardiac cycle. **RESULTS:** The timing of systolic CSF flow in the cervical subarachnoid space (SAS) correlated very closely to the brain arteriovenous blood flow difference during the cardiac cycle. This arteriovenous difference was a measure of brain expansion. Aqueduct CSF flow during the cardiac cycle differed from SAS flow in that systolic flow was delayed in comparison with systolic cervical SAS flow. The normal aqueductal oscillatory flow volume was 1.7 ± .4 mL/min or 0.03 ± 0.01 mL per cardiac cycle. This represented 14.5% ± 3.1% of the total CSF flow and tissue displacement through the incisura which was 14.5 ± 2.2 mL/min or 0.22 ± 0.03 mL per cycle. CSF oscillatory flow volume in the cervical SAS was 39.0 ± 4.0 mL/min or 0.65 ± 0.08 mL per cycle. **CONCLUSION:** CSF flow can be measured. Results in healthy subjects show relatively low oscillatory flow through the aqueduct which is slightly out of phase (delayed) compared with SAS CSF flow.

Index terms: Cerebrospinal fluid, flow dynamics; Cerebrospinal fluid, magnetic resonance; Magnetic resonance, flow studies

AJNR 14:1301–1307, Nov/Dec 1993

The development of motion-sensitive magnetic resonance (MR) pulse sequences has revived interest in the study of the third circulation, cerebrospinal fluid (CSF) flow (Ida M, Hata Y, Tada S, Abe T. *Cine MR imaging of cerebrospinal fluid flow in syringomelia*; and Itabashi T, Arai S, Kitahara H, Watanabe T, Suzuki H. *Quantitative analysis of cervical cerebrospinal fluid pulsation*. Abstracts of the 74th Annual Meeting of the Radiology Society of North America, Chicago, 1988) (1–9). These motion-sensitive pulse sequences have improved capabilities, allowing measurement of both velocity and direction of fluid motion (7–13). When combined with an area measurement, volume flow can be calculated. To date, most of the CSF physiology described by MR methodology has been descriptive and qualitative in nature (Ida and Itabashi cited above) (1–8). Velocities have been measured and the timing relationships of CSF flow in various portions of the neuraxis have been accurately characterized (Itabashi cited above) (1, 2). CSF flow has been measured mostly through the aqueduct (5–7).

The purpose of this investigation was to measure CSF flow between the major CSF compartments, the supratentorial and infratentorial compartments, and the spinal canal. The study was designed to provide normative data for movement of CSF between these three major compartments. From these data, it is hoped, CSF flow derangement can be quantified in the future.

Materials and Methods

This prospective study was carried out on a 1.5-T imager (Signa General Electric Medical Systems, Milwaukee, Wis) using a phase contrast cine MR pulse sequence which has been previously described (2, 13). Briefly, two cine acquisitions (14) interrogating the same section but with different sensitivity to velocity in the section select direction are interleaved. The strength of the velocity encoding is parametrized by V_{enc}, the velocity that produces a phase shift of 180° between the acquisitions. Stronger encoding

Received March 6, 1992; revision requested June 8; revision received January 27, 1993 and accepted February 8.

Both authors: Department of Radiology, Stanford University School of Medicine, Stanford, CA 94305-5105. Address reprint requests to Dieter R. Enzmann, MD, Department of Radiology, Room S-072, Stanford, CA 94305–5105.

AJNR 14:1301–1307, Nov/Dec 1993 0195-6108/93/1406–1301

(smaller V_{enc}) produces improved precision for measuring slow motions but accommodates a smaller range of velocities ($\pm V_{enc}$) before aliasing occurs. In the present study, V_{enc} was always selected so as to avoid velocity aliasing in regions within which quantitative measurements were being made. Pulse sequence repetitions are executed continuously and at a constant rate so as to maintain an MR equilibrium and to allow the entire cycle to be studied. Sequence repetitions within the same cardiac cycles use the same spatial phase-encoding gradient and alternating velocity sensitivity, and the phase-encoding amplitude is updated upon detection of a cardiac trigger. The data from each individual cardiac period for each velocity sensitivity are interpolated into the desired number of frames in the cardiac cycle. This phase-contrast cine method produces both conventional magnitude images and phase-contrast flow images, the former from the average of magnitude reconstruction of the two data sets at each point in time and the latter from the difference in phase images. For additional details of this phase-contrast cine technique see ref. 13.

The interleaved acquisition minimizes sensitivity to other motions (eg, respiration) but yields a temporal resolution of approximately twice the sequence repetition time. For this study, the technical parameters were: 54/9–13/2 (repetition time/echo time/excitations) yielding a temporal resolution of 108; matrix, 128 × 256; section thickness, 5 mm; field of view, 12 cm. The acquired raw data were interpolated to produce 16 frames equally spaced in the cardiac cycle. Two different velocity encoding ranges (V_{enc}) were used. A V_{enc} value of 15 cm/sec was for the aqueduct and C2–3 subarachnoid space (SAS) CSF flow. An oblique axial plane of section was selected to be perpendicular to the aqueduct (at the inferior colliculus) just above the fourth ventricle where its course is nearly vertical. In addition, the area of the aqueduct is largest in this region. This minimizes partial volume artifacts. Carotid and vertebral artery and jugular vein blood flow was measured at the same level as the C2–3 CSF scan but a V_{enc} of 150 cm/sec was used in an axial scan perpendicular to these vessels. These measurements were performed in 10 healthy volunteers, six men ages 26 to 36 years and four women ages 23 to 34 years. Peripheral gating was used in all cases. Although electrocardiographic gating might be preferred in general, it was not possible with the field of view and repetition time required in the present study due to excessive gradient interference corrupting the electrocardiogram signal. Thus, electrocardiographic gating was sacrificed to obtain improved spatial resolution. Further, peripheral gating was judged to be acceptable for the relative timing measurements envisioned in this study.

Phase-contrast cine produces images that represent velocity as a function of time in the cycle. Additive errors (baseline) may be present because of the effects of gradient-induced eddy currents, but these errors must be similar in neighboring regions. Before quantitative analysis of flow within any region of interest (ROI), a constant baseline for that region was estimated by the average throughout the cycle of the apparent velocity in a neighboring static structure. These baseline regions were chosen where brain motion is minimal or absent during the cardiac cycle; we have studied brain motion in detail. In addition, because the baseline measurements were averaged throughout the cardiac cycle and because there is no net brain motion, cyclical brain motion cannot corrupt the baseline estimate or alter the measured pulsatile waveforms.

For each pixel and each of the 16 time frames, the product of the velocity (apparent velocity − baseline) in the pixel and the pixel area is an estimate of the volume flow rate (milliliters per minute) through the pixel. Volume flow rate as a function of time through vessels or CSF spaces was measured as the sum of the volume flow rates through the pixels within a defined ROI for each frame. This measurement is relatively insensitive to pixel size, ROI size, and flow angulation (15). Nevertheless, the imaging plane was positioned perpendicular to the flow of interest to minimize partial volume effects. The average flow rate was measured by averaging the volume flow rate through the cycle, and was expressed as milliliters per minute, or as milliliters per cycle by dividing by the heart rate. The accuracy of average volume flow rate measurements has been validated in vitro (16) and in vivo (15).

For a given ROI and for any frame, the product of volume flow rate (milliliters per minute) and the time interval between cine frames (min) is the volume (milliliters) displaced through the ROI during that frame. The sum of this quantity over all frames in which it is positive is an estimate of the volume (milliliters) displaced in one direction through the ROI. A similar sum over negative values can be performed. The lesser of the two in absolute value represents the volume that is displaced in a reciprocating or oscillatory fashion through the ROI over one cycle (in units of milliliters per cycle, or milliliters per minute if multiplied by the heart rate).

Flow during the cardiac cycle was determined for the aqueduct (Fig 1) and the C2–3 SAS (Fig 2). At the incisura, the volume of tissue and the volume of CSF displaced through it were measured (Fig 3). In addition, an arterio-

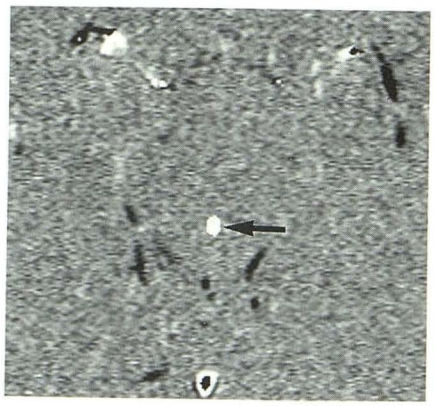

Fig. 1. Axial phase-contrast flow image of the midbrain showing the level at which aqueductal flow was measured. The white region in the dorsal midbrain (*arrow*) is the ROI drawn over the aqueduct and used for flow measurements. The aqueduct is seen as the white ROI (*arrow*) in the dorsal midbrain.

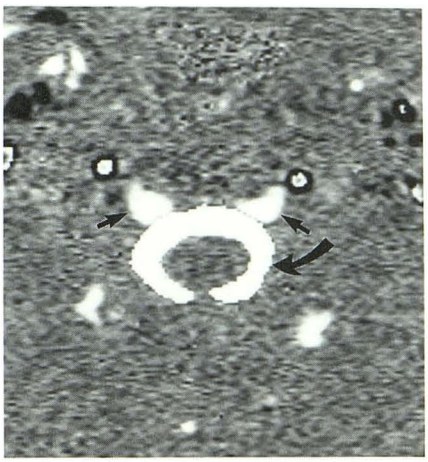

Fig. 2. Axial phase-contrast image of the cervical SAS at the C2–3 level. A white ROI is overlaid on the SAS (*curved arrow*) around the cervical cord. The two cuneiform structures (*straight arrow*) anterior to the SAS represent epidural venous sinuses with flow in the craniocaudal direction. Note that the neck vessels show a complex target pattern indicating flow aliasing because the V_{enc} for CSF flow was set at 15 cm/sec.

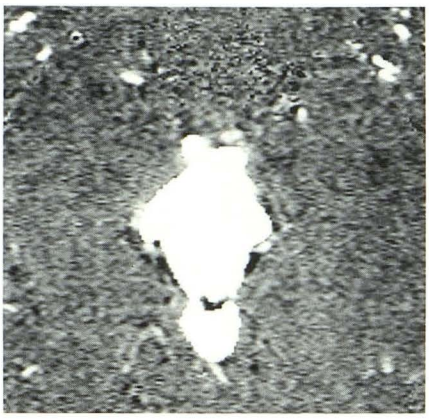

Fig. 3. Axial phase-contrast image through the midbrain at the level of the tentorium. Displacement of incisural tissue, brain and CSF, was measured by an irregular ROI that included all of the structures in the incisura including CSF and brain tissue. Vascular structures were excluded.

venous flow difference was calculated throughout the cardiac cycle. The flow in both internal carotid arteries and both vertebral arteries were added together to produce an arterial inflow curve. Flow in the right and left internal jugular veins was combined as a measure of venous outflow. This is likely to be an underestimate of the true venous outflow since other venous structures such as the pterygoid plexus and the ophthalmic vein were not taken into account. To correct for this, the measured venous curve was multiplied by a factor that forced the corrected average venous outflow to equal the average arterial inflow. On average, this scale factor was 1.37 and was equivalent to an underestimation of about 3.2 mL per cycle. The arteriovenous flow difference was calculated as the difference between the measured arterial curve and the scaled venous curve. Of particular interest in this study is the relative timing of this arteriovenous difference with respect to CSF flow. This relative timing is expected to be accurate in the face of underestimated venous outflow.

In the aqueduct, both the oscillatory flow volume and average (net) CSF flow rates were measured. The area of measurement ranged from 0.068 cm^2 to 0.136 cm^2 and comprised at least 13 pixels. Errors in measurement due to partial volume artifact were felt to be minimal because the section was oriented perpendicular to the aqueduct and the pixel size was small relative to the aqueduct. The flow measurement through the incisura contains components caused by motion of both CSF (interpeduncular cistern, perimesencephalic cistern, and superior vermian cistern) and brain tissue (ie, the midbrain, and sometimes the superior vermis). A V_{enc} of 15 cm/sec allowed measurement without aliasing. Blood vessels were always excluded from this ROI. ROI measurements were limited to the anatomic structure of interest (Fig 4). Although CSF flow information was derived from the phase contrast flow images, the ROIs for vascular blood flow measurements were drawn either on the flow image or the magnitude image, whichever allowed best depiction of the anatomic boundaries (Fig 4). Irregular ROIs were drawn to encompass the SAS at the C2–3 level (Fig 2). Volume flow rate curves were calculated for each of the following: the arteriovenous difference, C2–3 SAS aqueduct, and incisura. A ratio was used to compare average flow rates between major compartments: incisura flow divided by C2–3 SAS. This yields the fraction of total CSF flow displaced from the cranium arising from the supratentorial motion.

The measured data for all patients (flow as a function of phase in the cardiac cycle, arteriovenous difference, average flow rate, and flow ratios) were combined (see Fig 5 and Table 3). All measurements are presented as the mean ± SEM of all individuals.

Results

The temporal relationship between CSF flow in the cranial and spinal SAS and brain expansion, as measured by the arteriovenous flow difference, is shown in Figure 5. The arteriovenous difference, when superimposed on the C2–3 SAS curve, shows there is net intracranial inflow of blood during CSF systole and net outflow during CSF diastole. The onset of CSF systole in the C2–3 SAS and incisura occurs simultaneously with brain expansion and the increase in the arteriovenous flow difference (Fig 5). In this group of subjects CSF flow in the C2–3 SAS was simultaneous anterior and posterior to the cord. The flow pattern of CSF in the cervical SAS throughout the cardiac cycle corresponded closely to that of the arteriovenous flow difference (Fig 5). These data show a delay in CSF flow reversal in both systole and diastole in the

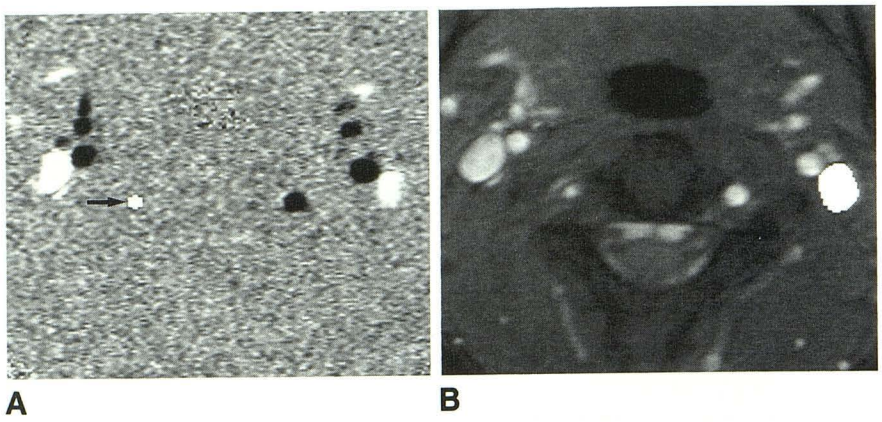

Fig. 4. *A*, Axial phase-contrast image of the major arteries and veins in the neck at the C2–3 level. V_{enc} = 150 cm/sec. The internal carotid arteries and both vertebral arteries are depicted as black while the internal jugular veins are seen as white. A white region of interest (ROI) (*arrow*) is superimposed on the right vertebral artery.

B, Corresponding magnitude image depicts the vasculature, arteries and veins, as high signal. This image shows a white ROI superimposed on the left internal jugular vein.

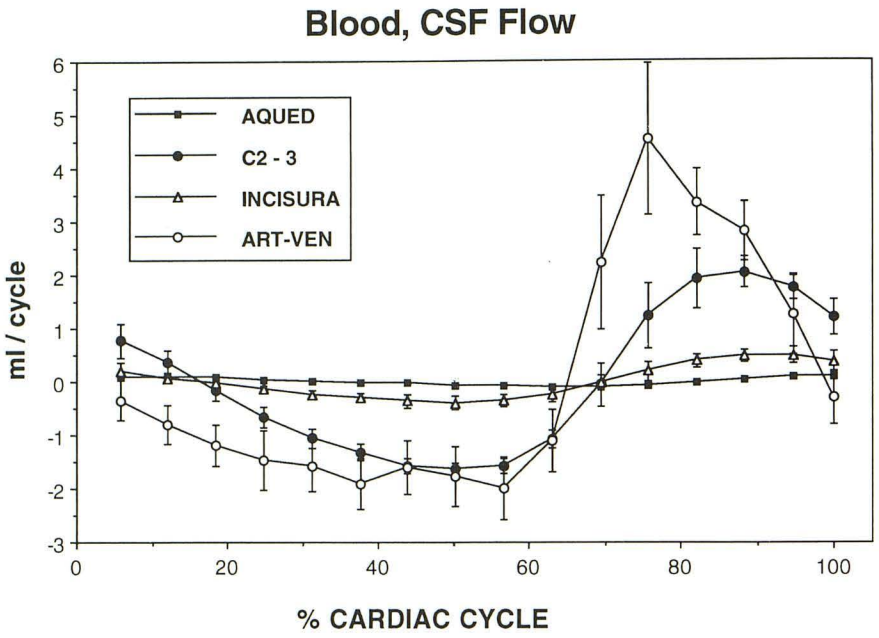

Fig. 5. Mean volume flow (all the volunteers) during the cardiac cycle defined by a peripheral pulse trigger. Arteriovenous flow difference (ART-VEN), cervical SAS CSF flow (C2–3), and incisura and tissue displacement (INCISURA) show a close correlation. SAS flow reversal and systolic CSF flow follow the steep rise in arteriovenous flow difference. Incisura CSF flow and tissue displacement have a profile nearly identical to C2–3 showing systolic flow reversal to be simultaneous. Aqueductal CSF flow (AQUED) is out of phase with C2–3 and INCISURA flow, being delayed in both systolic and diastolic reversal of flow.

TABLE 1: Vascular Blood Flow

	Mean ± SEM (mL/min)	Mean ± SEM (mL/cycle)
Carotid		
R	305 ± 21	5.17 ± 0.43
L	288 ± 24	4.87 ± 0.55
Vertebral		
R	97 ± 17	1.65 ± 0.31
L	131 ± 16	2.23 ± 0.31
Jugular		
R	338 ± 56	5.74 ± 1.13
L	293 ± 49	4.97 ± 1.05

Note.—R indicates right, L, left.

aqueduct compared with CSF flow in the SAS. Aqueduct flow was still in a cranial direction (diastolic flow) when C2–3 CSF flow is already in a caudal (systolic) direction.

The average blood flow rates in the carotid and vertebral arteries and jugular veins are listed in Table 1, whereas Tables 2 and 3 contain the measured CSF flow rates and resultant ratios. The normal aqueductal oscillatory volume flow (volume flow during systole) is low, being 1.7 ± 0.4 mL/min or 0.03 ± 0.01 ml per cardiac cycle (Table 2). The net aqueductal flow (ie, CSF production) was calculated to be 0.4 ± 0.12 mL/min in this group of 10 healthy subjects. Net CSF flow through the aqueduct was 22 ± 8% of the aqueductal oscillatory volume flow in this normal group. The volume of CSF and brain tissue displaced through the incisura was measured to be

TABLE 2: CSF Flow

	mL/min	mL/cycle
Aqueduct		
Stroke volume	1.7 ± 0.4	0.03 ± 0.01
Net flow	0.40 ± 0.12	
Incisura	14.5 ± 2.2	0.22 ± 0.03
C2-3	39.0 ± 4.0	0.65 ± 0.08

TABLE 3: Flow Ratios

Aqueduct/incisura	14.5% ± 3.1
Incisura/C2-3	41% ± 7.8

14.5 ± 2.2 mL/min or 0.22 ± 0.03 mL per cycle (Table 2). The average ratio of aqueduct oscillatory CSF flow volume to total incisural CSF flow and brain displacement was 14.5 ± 3%. Thus, CSF displacement throughout the aqueduct is only a small portion of the CSF and tissue displaced from the supratentorial compartment through the incisura to accommodate supratentorial brain expansion.

CSF oscillatory flow volume at the C2–3 SAS level was measured to be 39 ± 4 mL/min or 0.65 ± 0.08 mL per cycle, exceeding that through the incisura. The ratio of incisural to C2–3 SAS volume displacement was 41 ± 8% for this healthy group (Table 3). This indicates that approximately 40% of the volume of CSF displaced into the spinal canal relates to supratentorial brain expansion and 60% to infratentorial brain expansion.

Discussion

These data suggest that the primary driving force behind intracranial and spinal canal CSF flow is expansion of the brain during vascular systole. The timing and approximate degree of brain volume expansion can be estimated from the measured difference between simultaneous arterial inflow and venous outflow from the intracranial space during the cardiac cycle (ie, the arteriovenous difference). Since arterial inflow and venous outflow are not equal throughout the cardiac cycle, there is a short period of brain expansion during vascular systole. By measuring total arterial input from the internal carotid and vertebral arteries and simultaneous venous outflow in the internal jugular veins, one can obtain an upper limit of this arteriovenous difference because outflow through the ophthalmic veins, pterygoid plexus, and other routes is not taken into consideration. Flow through these other venous channels, however, is expected to be small compared with that in the jugular veins and, if flow through them is assumed to be similar to that in the internal jugular veins, then the arteriovenous difference can be corrected so that the net flow during a cardiac cycle is zero. In any case, the measured relative timing of this arteriovenous flow difference to CSF flow should be accurate. The very close correlation between the time course of the arteriovenous flow difference and C2–3 SAS CSF flow supports a causal relationship. C2–3 CSF flow represents the net amount of displaced CSF from the intracranial cavity resulting from brain expansion. The steep rise in the arteriovenous difference in vascular systole (ie, overall brain expansion) coincides with the onset of caudal (systolic) CSF flow in the cervical SAS. The time course of SAS CSF flow and brain stem motion through the incisura is similar, again suggesting a direct relationship to brain expansion (17, 18). Brain motion studies have shown caudal displacement of the brain stem at the onset of systole, and this presumably is the force behind local CSF motion (17, 18). Brain motion, however, is not simultaneous and supratentorial brain expansion would be expected to follow infratentorial expansion as the vascular systolic peak is delayed in the middle cerebral artery compared with the basilar artery (19). Caudal flow (systolic) in the aqueduct, however, is delayed in time compared with that in the SAS. During the onset of brain expansion, CSF flow in the aqueduct is still in a cranial direction (ie, diastolic). The time delay of CSF oscillation in the aqueduct possibly results from aqueductal flow being governed not by local midbrain motion but by ventricular flow, which, in turn, results from supratentorial brain expansion.

Displacement of tissue through the incisura is an additional mechanism available to accommodate supratentorial brain expansion. Displacement of both midbrain tissue and CSF through the incisura is on the order of 0.22 mL per cardiac cycle, approximately 40% of the total CSF flow that is ultimately displaced into the spinal canal. Therefore, 60% of the CSF displaced into the spinal canal arises from expansion of posterior fossa structures. The total volume of CSF displaced from the intracranial space into the spinal canal is 39 mL/min or 0.65 mL per cardiac cycle. This represents the volume of brain expansion not accommodated by intracranial capacitance.

It seems counterintuitive to have a greater portion of the displaced intracranial volume arise from the posterior fossa and a smaller volume from the larger supratentorial space. However, the difference in proportion may simply mean that supratentorial brain expansion can be accommodated by means other than CSF displacement such as by compression of venous structures or expansion through structures such as the orbital fissures. These proportions do not mean there is greater expansion of posterior fossa brain tissue.

The normal CSF aqueductal oscillatory flow volume is small, on the order of 1.68 mL/min or 0.03 mL per cardiac cycle. This is a small percentage of the total CSF and brain tissue displaced from the supratentorial compartment into the infratentorial compartment during vascular systole. Under normal circumstances, therefore, CSF displacement from the lateral and third ventricles is a minor mechanism for accommodating cyclical brain expansion. CSF production calculated from this group of healthy individuals falls within the range published previously (20–22).

The phase-contrast cine technique used in this study would benefit from additional technical advances. The temporal resolution of the measurements would be improved by a shortening of repetition time. Inadequate temporal resolution will smooth the flow curves but not degrade average flow measurements or alter relative timing relationships. The present temporal resolution is believed to be adequate for CSF flow measurements. The lower range of velocities that can be measured by phase-contrast techniques can be limited by unwanted phase shifts caused by eddy currents. The resulting additive errors can have significant impact on measured volume flow rates through large ROIs, such as the incisura. In the present study these effects were mitigated by the use of corrections based on apparent velocities in static structures. Because there is no net motion of brain, its average velocity must be zero. A further limitation is imposed by the noise in the velocity images, which is in turn dependent on the image signal-to-noise ratio and the flow encoding strength (V_{enc}) (23). This noise limit is particularly relevant in small anatomic structures, such as the aqueduct. For these measurements, even stronger flow encoding (smaller V_{enc}) would be helpful. Partial volume errors can result in falsely high volume flow rates. Perpendicular imaging plane positioning minimized this potential source of error. Thinner sections and higher spatial resolution would reduce partial volume effects and facilitate ROI definition. Although this would be beneficial for small structures (eg, aqueduct), image and flow signal-to-noise ratios would be degraded and, in our present implementation, this would be accompanied by a severe penalty in repetition time and echo time. The cine phase contrast technique as used provided consistent quantitative data for the normal population examined.

References

1. Feinberg DA, Mark AS. Human brain motion and cerebrospinal fluid circulation demonstrated with MR velocity imaging. *Radiology* 1987;163:793–799
2. Enzmann DR, Pelc NJ. Normal flow patterns of intracranial and spinal cerebrospinal fluid defined with phase-contrast cine MR imaging. *Radiology* 1991;178:467–474
3. Quencer RM, Donovan MJ, Hinks RS. Cine MR in the evaluation of normal and abnormal CSF flow: intracranial and intraspinal studies. *Neuroradiology* 1990;32:371–391
4. Levy LM, Di Chiro G. MR phase imaging and cerebrospinal fluid flow in the head and spine. *Neuroradiology* 1990;32:399–406
5. Mascalchi M, Ciraolo L, Bucciolini M, Inzitari D, Arnetoli G, Dal Pozzo G. Fast multiphase MR imaging aqueductal CSF flow. II. Study in patients with hydrocephalus. *AJNR: Am J Neuroradiol* 1990;11:597–603
6. Ciraolo L, Mascalchi M, Bucciolini M, Dal Pozzo G. Fast multiphase MR imaging of the aqueductal CSF flow. I. Study of healthy subjects. *AJNR: Am J Neuroradiol* 1990;11:589–596
7. Thomsen C, Stahlberg F, Stubgaard M, Nordell B. The Scandinavian Flow Group. Fourier analysis of cerebrospinal fluid velocities: MR imaging study. *Radiology* 1990;177:659–665
8. Bradley WG, Kortman KE, Burgoyne DE. Flowing cerebrospinal fluid in normal and hydrocephalic states: appearance on MR images. *Radiology* 1986;159:611–616
9. Sherman JL, Citrin CM, Brown BJ, Gangarosa RE. MR demonstration of altered cerebrospinal fluid flow by obstructive lesions. *AJNR: Am J Neuroradiol* 1986;7:571–579
10. Nayler GL, Firmin DN, Longmore DB. Blood flow imaging by cine magnetic resonance. *J Comput Assist Tomogr* 1986;10:5:715–722
11. Firmin DN, Nayler GL, Klipstein RH, Underwood SR, Rees RSO, Longmore DB. In vivo validation of MR velocity imaging. *J Comput Assist Tomogr* 1987;11:751–756
12. Spritzer CE, Pelc NJ, Lee JN, Evans A, Sostman HD, Riederer SJ. Preliminary experience with rapid MR blood flow imaging using a phase sensitive limited flip angle gradient refocused pulse sequence. *Radiology* 1990;176:255–262
13. Pelc NJ, Herfkens RJ, Shimakawa A, Enzmann DR. Phase contrast cine magnetic resonance imaging. *Magn Res Quarterly* 1991;7:229–254
14. Glover GH, Pelc NJ. A Rapid Cine MRI Technique. In: Kressel H, ed. *Magnetic resonance annual 1988.* New York: Raven, 1988
15. Pelc LR, Pelc NJ, Rayhill SC, et al. Arterial and venous blood flow: noninvasive quantification with MR imaging. *Radiology* 1992;185: 808–812
16. Evans AJ, Iwai F, Grist TA, et al. MR imaging of blood flow with a phase subtraction technique: in vitro and in vivo validation. *Invest Radiol* 1993;28:109–115
17. Enzmann DR, Pelc NJ. Brain motion: measurement with phase-contrast MR imaging. *Radiology* 1992;185:653–660

18. Poncelet BP, Wedeen VJ, Weisskoff RM, Cohen MS. Brain parenchyma motion: measurement with cine echo-planar MR imaging. *Radiology* 1992;185:645–651
19. Enzmann DR, Ross MR, Marks MP, Pelc NJ. Blood flow in major cerebral arteries measured by phase contrast cine MR. *AJNR: Am J Neuroradiol* (in press)
20. Milhorat TH. The third circulation revisited. *J Neurosurg* 1975;42:628–645
21. Rottenberg DA, Howieson J, Deck MD. The rate of CSF formation in man: preliminary observations on metrizamide washout as a measure of CSF bulk flow. *Ann Neurol* 1977;2:503–510
22. Cutler RWP, Page L, Galicich J, Watters GV. Formation and absorption of cerebrospinal fluid in man. *Brain* 1968;91:707–720
23. Pelc NJ, Bernstein MA, Shimakawa A, Glover GH. Encoding strategies for three-direction phase-contrast MR imaging of flow. *J Magn Reson Imaging* 1991;1:405–413

Please see the Commentary by McComb on page 1309 in this issue.